AIChE WILEY InterScience DISCOVER SOMETHING GREAT

PROCESS SYSTEMS ENGINEERING

Designing Man-Portable Power Generation Systems for Varying Power Demand

Mehmet Yunt
Dept. of Mechanical Engineering, Massachusetts Institute of Technology, Cambridge, MA 02139

Benoît Chachuat
Laboratoire d' Automatique, École Polytechnique Fédérale de Lausanne, Lausanne, Switzerland

Alexander Mitsos and Paul I. Barton
Dept. of Chemical Engineering, Massachusetts Institute of Technology, Cambridge, MA 02139

DOI 10.1002/aic.11442
Published online March 31, 2008 in Wiley InterScience (www.interscience.wiley.com).

Portable electronic devices operate at varying power demand levels. This variability of power demand must be considered explicitly in the design of man-portable power generation systems for acceptable performance and portability. In this regard, a mathematical programming based design method is proposed. The method transcribes optimal operation of the system at a given power demand into a mathematical program. The power demand specific programs are incorporated into another upper level mathematical program encoding design requirements to form a final two-stage formulation. The design and operational parameters of the power generation system comprise a solution of the formulation. Unlike designs, based on a nominal power demand, the design guarantees that each power demand and all operational requirements can be satisfied. A detailed study of a microfabricated fuel-cell based system is performed. The proposed method produces smaller designs with significantly better performances than nominal power demand based approaches. © 2008 American Institute of Chemical Engineers *AIChE J,* 54: 1254–1269, 2008
Keywords: optimization, man-portable power, micro fuel cell, micro-SOFC, intermediate-fidelity modeling

Introduction

Batteries are currently the predominant portable power source for electronic devices. They are widely available, robust and easily usable. However, they cannot adequately meet the ever-increasing power demand driven by the widespread use of portable electronic devices in military and civilian applications. The available energy that can be stored in a battery per unit volume (*volumetric energy density*) or unit mass (*gravimetric energy density*) is on the order of a few hundred Wh/l or Wh/kg, respectively.[1,2] Compared to the fuel energy densities of chemical fuels, these values are significantly lower. Common battery materials are toxic and provisions need to be made to collect depleted batteries for safe disposal and recycling. Moreover, the scope for future performance improvements is small. Most active battery material candidates of practical value have already been investigated and the list of unexplored materials is being depleted.[1,3]

Correspondence concerning this article should be addressed to P. I. Barton at pib@mit.edu.

© 2008 American Institute of Chemical Engineers

Microturbines,[4] thermophotovoltaic cells,[5] and microfabricated fuel cells[6] are some of the candidate alternative technologies for portable power generation systems that operate for longer durations without recharging, refilling or replacement. Microfabricated fuel cell based systems are the main focus of this article. These systems produce electricity by electrochemical oxidation of common high-energy-content fuels and chemicals, such as hydrocarbons and alcohols. Potentially, power generation systems with significantly higher-energy densities than those of state-of-the-art batteries can be conceived.

Fabrication of miniature components is necessary to create high-energy-density fuel cell systems. In this regard, promising advances in the fabrication of microchemical reactors and fuel cells have been made.[7–9] Miniature components have also been modeled.[10–12]

Not only the fabrication and modeling of each component, but also careful system design is necessary to obtain superior performance from a microfabricated fuel cell.[13] Microscale and macroscale process design are significantly different. In microscale design, tight spatial integration of components necessitates the simultaneous consideration of component layout and process selection. Heat management is harder due to spatial constraints and a shortage of applicable technologies. Portability, safety and autonomous operation requirements are more stringent.

Various process design aspects of microfabricated fuel-cell systems have been investigated in the literature. A superstructure representing plausible process alternatives has been proposed.[13] The superstructure has been used to make comparisons between different processes, as well as to study the effect of heat losses, scale, fuel efficiency and conversion. Layout options have been investigated within the superstructure approach.[14]

The purpose of these system-level considerations has been to analyze the performance of a multitude of candidate processes without detailed modeling of components. Electrochemical efficiencies and conversions, that theoretically can be calculated from detailed models, are inputs supplied by the designer. Inherently, this approach is not suitable to study directly the effect of parameters such as operating temperatures that affect the device performance through intricate and multiple mechanisms.

In order to analyze the effect of physical parameters on a micro fuel cell design, the *intermediate-fidelity* modeling method has been developed.[15] Unlike the superstructure-based method, the intermediate-fidelity modeling method allows the calculation of efficiencies and conversions from first principles. Under reasonable and justified assumptions, a reduction in modeling complexity can be achieved by only representing spatial variations of quantities in a single dimension along the length of the channels, or even lumping certain quantities, such as temperature. It has been demonstrated that this approach results in sufficiently detailed models to investigate effectively the sensitivity of system performance to power demand, operating temperature and physicochemical parameters, without resorting to computationally expensive computational fluid dynamics (CFD) methods. A mathematical programming based method has been introduced to design a system to meet a single power demand at steady state based on this intermediate-fidelity modeling approach. The dynamic behavior during startup of a fuel-cell system coupled with a battery has also been investigated.[16,17]

In this study, varying power demands are incorporated into the mathematical programming design approach.[15] Most portable electronic devices do not operate at a constant power demand. Not only the magnitudes, but also the durations of operation at different power levels vary. Cellular phones on standby expend only a small fraction of the power needed during a conversation. The power demand of portable computers can range between 5 W and 30 W depending on usage.[18] The electronic equipment of the dismounted soldier is expected to require 20 W of power with a peak demand of 50 W.[19]

For varying power demand, constraints need to be satisfied and performance needs to be evaluated over a range of operating conditions. A design based on a single nominal power demand does not guarantee that the demand, in addition to stringent requirements on the operation of the device stemming from reliability and safety considerations, can be met for multiple power levels.

In the remainder of this article, a method is proposed to incorporate varying power demand operation into a mathematical program where the underlying chemical process is modeled using the intermediate-fidelity modeling approach. A detailed case study is presented demonstrating the superiority of the proposed method over other possible design methods.

Method to Design Micropower Generation Systems for Varying Power demand

A mathematical programming based design approach is presented in this section. The goals and requirements of the design are transcribed into the objective function and constraints of an optimization problem. Parameters of the design, e.g., reactor volumes, material flow rates and operating temperatures, are obtained as solutions of the optimization problem.

The proposed mathematical program contains two classes of decision variables: *operational decision variables* and *design decision variables*. Design decision variables represent properties of the system that cannot be altered after fabrication of the device, e.g., reactor volumes. Operational decision variables represent properties of the system that can be adapted to the current power demand, e.g., operating temperature, cell voltage and flow rates.

In the case of varying power demand, optimal operational variables need to be determined for each possible demand. In order to optimize operational decision variables, a mathematical program is formulated for each possible power demand. These power demand specific mathematical programs amount to constraints that ensure optimal device operation in accordance with operational constraints. The solution of each of these programs determines operational decisions for the corresponding demand as a function of the design decision variables. Another mathematical program encodes design requirements on the fabrication of the device. The set of power demand specific mathematical programs is incorporated into this mathematical program as constraints in order to obtain a final two-stage optimization formulation.

In this article, only the steady-state power demand on the microfabricated fuel-cell system is considered. The perform-

ance penalty incurred by switching from one power output level to another is assumed to be negligible, as well as the duration of transient operation compared to steady-state operation. These assumptions are motivated by the fact that fuel-cell based power generation systems are not responsive enough to meet rapid demand changes. Batteries and/or supercapacitors need to be deployed to work in tandem to overcome this deficiency. In such hybrid electrochemical systems, microfabricated fuel-cell based systems are intended to operate mostly at steady state.[19]

In order to formulate the mathematical program, a finite number of possible power demands $\mathcal{P}_i$, and frequencies of occurrence p_i, for each possible power demand during the time frame of interest (a.k.a. the mission) must be specified, with $i \in \mathcal{I} \equiv \{1,\ldots,N_d\}$. For each power demand and given values of the design decision variables, optimal operational decision variables are determined as a solution of the mathematical program

$$\begin{aligned} Q_i(\mathbf{x},\mathcal{P}_i) \equiv \min_{\mathbf{y}_i} \quad & f^{(2)}(\mathbf{x},\mathbf{y}_i,\mathcal{P}_i) \\ \text{s.t.} \quad & \mathbf{0} \geq \mathbf{g}^{(2)}(\mathbf{x},\mathbf{y}_i,\mathcal{P}_i) \\ & \mathbf{0} = \mathbf{h}^{(2)}(\mathbf{x},\mathbf{y}_i,\mathcal{P}_i) \\ & \mathbf{y}_i \in Y \end{aligned} \qquad (\mathrm{L_i})$$

where Q_i is the solution value of the program; $\mathcal{P}_i$ is a possible power demand; $\mathbf{x}$ represents the design decision variables; $\mathbf{y}_i$ represents the operational decision variables corresponding to operation at power level $\mathcal{P}_i$; $f^{(2)}$ represents the objective to be minimized at each power demand level; and $\mathbf{g}^{(2)}$ and $\mathbf{h}^{(2)}$ represent constraints on the operation of the system, and Y represents bounds on the possible values of the operational decision variables.

The constraints of (L_i) represent safety, reliability and efficiency requirements on the operation of the system. The constraints ensure that for a given power demand, the optimal decisions result in sufficient production of power to meet that demand. In addition, the constraints embody the governing equations of the chemical, electrical and mechanical phenomena of the micropower generation system. The objective $f^{(2)}$ represents the cost of operation to meet a single power demand, e.g., fuel expenditure, gravimetric and volumetric energy densities.

Each program (L_i) is incorporated into the top level program

$$\begin{aligned} \min_{\mathbf{x}} \quad & f^{(1)}(\mathbf{x}) + \sum_{i=1}^{N_d} p_i Q_i(\mathbf{x},\mathcal{P}_i) \\ \text{s.t.} \quad & \mathbf{0} \geq \mathbf{g}^{(1)}(\mathbf{x}) \\ & \mathbf{0} = \mathbf{h}^{(1)}(\mathbf{x}) \\ & \left.\begin{aligned} Q_i(\mathbf{x},\mathcal{P}_i) = \min_{\mathbf{y}_i} \quad & f^{(2)}(\mathbf{x},\mathbf{y},\mathcal{P}_i) \\ \text{s.t.} \quad & \mathbf{0} \geq \mathbf{g}^{(2)}(\mathbf{x},\mathbf{y}_i,\mathcal{P}_i) \\ & \mathbf{0} = \mathbf{h}^{(2)}(\mathbf{x},\mathbf{y}_i,\mathcal{P}_i) \\ & \mathbf{y}_i \in Y \end{aligned}\right\} \forall i \in \mathcal{I} \\ & \mathbf{x} \in X, \end{aligned} \qquad (\mathrm{M})$$

where $f^{(1)}(\mathbf{x})$ represents a cost dependent only on the design variables, e.g., weight or volume of the power generation device; $\mathbf{h}^{(1)}$, $\mathbf{g}^{(1)}$ and X are constraints on the design decision variables only; and p_i represents the frequency of occurrence of $\mathcal{P}_i$ during the mission duration with $\sum_{i=1}^{N_d} p_i = 1$. The objective to be optimized consists of a weighted sum of the power demand specific program objective values, and a cost incurred by only the design variables. It represents a cost consisting of setup costs $f^{(1)}$, and operating costs Q_i, during a mission.

The formulation (M) assumes that each power demand occurs during a mission. This is the case when the performance of a device is appraised by means of standardized power demand profiles. For such demand profiles, the number of times the demand switches from a particular value to another particular value is known. In this case, the cost of each demand switch can easily be incorporated into the mathematical program as additional elements of the objective.

If power demand is interpreted as a random variable, it can be posited that only one or some of its possible values will occur during a mission. Then, (M) corresponds to a two-stage stochastic program with recourse.[20,21] In this case, the design decision variables correspond to first-stage variables and operational decision variables correspond to second-stage variables. The power demand specific programs (L_i) are called second-stage programs. The final two-stage program (M) is called the first-stage program. The choice of objective functions is restricted for (M) if power demand is considered as a random variable. Recourse programs are intended to optimize the expected value of the cost. The final solution of the recourse program optimizes the expected behavior of the microfabricated power generation system over many missions. In contrast, the two-stage mathematical program (M), can be used to optimize any quantity related to the performance of the power generation system in addition to the expected performance over a mission duration.

In principle, obtaining a solution to (M) requires the solution of each (L_i) as a function of $\mathbf{x}$. In some cases, analytical expressions for the (L_i) solutions can be obtained, simplifying the solution process for (M). In general, a solution of (M) is obtained by solving a related single-stage program

$$\begin{aligned} \min_{\mathbf{x},\mathbf{y}} \quad & f^{(1)}(\mathbf{x}) + \sum_{i=1}^{N_d} p_i f^{(2)}(\mathbf{x},\mathbf{y}_i,\mathcal{P}_i) \\ \text{s.t.} \quad & \mathbf{0} \geq \mathbf{g}^{(1)}(\mathbf{x}) \\ & \mathbf{0} = \mathbf{h}^{(1)}(\mathbf{x}) \\ & \left.\begin{aligned} & \mathbf{0} \geq \mathbf{g}^{(2)}(\mathbf{x},\mathbf{y}_i,\mathcal{P}_i) \\ & \mathbf{0} = \mathbf{h}^{(2)}(\mathbf{x},\mathbf{y}_i,\mathcal{P}_i) \\ & \mathbf{y}_i \in Y \end{aligned}\right\} \forall i \in \mathcal{I} \\ & \mathbf{y} \equiv (\mathbf{y}_1,\ldots,\mathbf{y}_{N_d}) \\ & \mathbf{x} \in X. \end{aligned} \qquad (\overline{\mathrm{M}})$$

The solution sets of (M) and ($\overline{M}$) are identical. The proof of equivalency is given in the appendix. Applicable numerical techniques to obtain a solution of ($\overline{M}$) depend on the

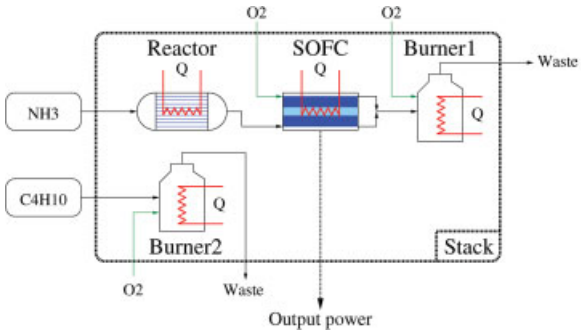

Figure 1. Process flowsheet.

[Color figure can be viewed in the online issue, which is available at www.interscience.wiley.com.]

structure of the constraint and objective functions and the decision variables (continuous and/or discrete).

The rest of the article describes an application of the proposed method to the design a microfabricated fuel cell stack to provide power up to 50.0 W. The performance of the resultant design is compared to the outcomes from other possible design approaches.

Design of a Microfabricated Fuel-Cell Stack

A fuel-cell system microfabricated into a silicon stack is designed using the proposed two-stage optimization method. The unit operation volumes, stack temperature, operating voltage and optimal chemical flow rates are determined using the proposed method.

The successful decomposition of NH_3 in microfabricated reactors with high-conversions[22,23] motivates the choice of NH_3 as the hydrogen source for demonstrative purposes. In addition, NH_3 is a fuel under consideration for possible military applications.[24] Combustion of C_4H_{10} provides the necessary additional heat for the endothermic catalytic decomposition of NH_3, and balances the heat losses to the ambient.

The process is arranged in two lines (Figure 1). The Ammonia line begins with a reactor for the catalytic decomposition of NH_3. The decomposition produces H_2 and N_2. A solid oxide fuel cell (SOFC) produces electricity from the oxidation of H_2. H_2 and N_2 are fed to the SOFC anode and air is fed to the cathode. The anode and cathode effluents pass to Burner I. The oxidation of unused hydrogen, and the decomposition of residual NH_3 takes place in this burner. The Butane line consists of Burner II for C_4H_{10} combustion. In total, there are four unit operations; two burners, a reactor, and an SOFC.

The inputs to the system are NH_3, C_4H_{10} and air at atmospheric pressure and 300K. The effluents of the system are NH_3, NO, O_2, N_2, CO_2 and steam at atmospheric pressure. The temperature of the effluents depends on the design.

The intermediate-fidelity model of this process has been published in prior work including the necessary data for reproduction and justification of assumptions.[15,25] A brief summary of the model is included, hereafter, with emphasis on the differences between the model used in this study and that in prior work.[15]

The intermediate-fidelity model is used to formulate constraints on the steady-state operation of the micro fuel-cell system in the context of the proposed design method. Power output, heat losses and mole fractions of reactants as a function of design decisions are obtained via this model.

Micro Fuel-Cell Stack Model

The model assumes that:

- the gas phase is ideal;
- the pressure inside the stack is uniform and equals atmospheric pressure;
- the stack operates at a spatially uniform temperature T;
- molar flux in the gas channels of the reactors is convective in the flow direction;
- axial diffusion and radial gradients are negligible.

Based on these assumptions, the mass and species conservation equations for each unit operation can be written as that of a plug-flow-reactor (PFR) at steady state[26]

$$\frac{dF}{d\eta} = V\sum_{j=1}^{n_r}\sum_{k\in\mathcal{J}_c} v_{i,j}r_j,$$
$$\frac{dz_i}{d\eta} = \frac{V}{F}\sum_{j=1}^{n_r}\left[v_{i,j} - z_i\sum_{k\in\mathcal{J}_c} v_{k,i}\right]r_j, \quad i\in\mathcal{J}_c, \tag{1}$$

where $\eta \in [0,1]$ is the dimensionless coordinate in the flow direction; F is the total molar flux, V is the volume of the unit operation; z_i is the mole fraction of species i; r_j is the rate of reaction j; $v_{i,j}$ is the stoichiometric coefficient for species i in reaction j; $\mathcal{J}_c \equiv \{NH_3, C_4H_{10}, N_2, H_2O, O_2, NO, CO_2\}$ is the set of species, and n_r is the number of reactions.

The model describes the fuel-cell stack behavior via a system of multistage differential-algebraic equations (DAEs)[27] with the unit operations corresponding to the stages. Each unit operation is described by a different set of equations of the general form Eq. (1). The solutions of the equations for each unit operation are coupled. In the Ammonia line, the mole fractions at the exit of the reactor affect the initial conditions for the set of equations describing the SOFC. Similarly, the mole fractions at the exit of the SOFC are the initial conditions for the set of equations describing Burner I. In addition to differential equations, the model contains algebraic equations to calculate the power output, heat losses, reaction rates and stack temperature. The Butane line equations are coupled to the Ammonia line equations by the overall energy balance for the stack.

The unit operations of the stack and design parameters are:

- **Ammonia Line:**

1. **Reactor:** NH_3 is endothermically decomposed using a catalyst according to

$$NH_3 \rightarrow \frac{3}{2}H_2 + \frac{1}{2}N_2$$

The reactor volume V^{b_I}, is the design decision variable. The optimal NH_3 inlet flow rate F^{r}_{in}, needs to be determined for each possible demand.

2. **SOFC:** The solid oxide fuel cell consists of a cathode and an anode that are separated by a solid electrolyte. At the cathode, oxygen from the air is converted to oxygen ions. The oxygen ions migrate to the anode through the ion-conducting

electrolyte. At the anode, hydrogen reacts with oxygen ions to produce water. Electrons flow back to the cathode via an external circuit. The half cell reactions of the process are

$$\text{cathode: } \frac{1}{2}O_2 + 2e^- \rightarrow O^{2-}$$
$$\text{anode: } H_2 + O^{2-} \rightarrow H_2O + 2e^-$$

$\mathcal{P}^{fc}$ is the power produced by the fuel cell. The volume of the fuel cell V^{fc}, is a design decision variable. The air inlet flow rate $F_{\text{in}}^{\text{ca}}$, and the fuel cell voltage U, need to be determined for each possible power demand.

3. **Burner I:** The SOFC effluents contain residual H_2 and NH_3. The oxidation of H_2 can provide heat to the endothermic decomposition of NH_3 in the reactor, as well as heat to balance heat losses. NH_3 is decomposed and both NH_3 and H_2 are oxidized using catalysts according to

$$NH_3 + \frac{5}{2}O_2 \rightarrow NO + \frac{3}{2}H_2O$$
$$NH_3 + \frac{3}{2}NO \rightarrow \frac{5}{4}N_2 + \frac{3}{2}H_2O$$
$$NH_3 \rightarrow \frac{1}{2}N_2 + \frac{3}{2}H_2$$
$$H_2 + \frac{1}{2}O_2 \rightarrow H_2O.$$

At the temperatures of operation of the fuel cell, the unimolecular decomposition of NO is not experimentally observed, hence, it is ignored in the model. Water, NH_3, NO, N_2 and O_2 comprise the effluents of the ammonia line. NH_3 and NO are toxic. The corresponding mole fractions in the effluent, $z_{NH_3}^{b_I}$ and $z_{NO}^{b_I}$, need to be kept low at safe levels. For example, the U.S. Department of Labor Occupational Safety and Health Administration (OSHA), imposes maximum discharge concentrations of 50 ppm and 25 ppm for NH_3 and NO, respectively.[28,29]

The design decision variable is the burner volume V^{b_I}. The operational decision variable is the burner inlet air flow rate $F_{\text{in}}^{b_I}$. The limits on the effluent concentration of NH_3 and NO are requirements that need to be met by the proposed design method for each power demand.

- **Butane Line:**

1. Burner II: The combustion of C_4H_{10} supplies the necessary heat for the endothermic decomposition of NH_3 and balances heat losses to the ambient. In prior work, a lumped model based on global mass and species balances represented Burner II.[15] Combustion was assumed to occur to fixed conversion irrespective of the burner volume.

In this study, a one-dimensional (1-D) PFR model for Burner II is used to account for the effect of the burner volume on conversion. The model consists of mass and species conservation equations of the form Eq. (1).

A premixed butane/air mixture is fed to the burner. The combustion of butane occurs using excess air with an oxygen stoichiometry value of 1.2. Butane combustion is modeled as a homogeneous irreversible, one-step reaction

$$C_4H_{10} + \frac{13}{2}O_2 \rightarrow 4\,CO_2 + 5\,H_2O$$

As a first approximation,[30] the reaction rate $r^{b_{II}}$ [mol·m^{-3}·s^{-1}] is calculated by

$$r^{b_{II}}(\eta) = k_0^{b_{II}} e^{\frac{-\mathcal{E}^{b_{II}}}{RT}} \left(z_{C_4H_{10}}^{b_{II}}(\eta)\right)^{0.15} \left(z_{O_2}^{b_{II}}(\eta)\right)^{1.6} \left(\frac{\rho^{b_{II}}}{10^6}\right)^{0.75}$$

where $\rho^{b_{II}}$ [mol·m^{-3}] is the total molar density in burner II (gas-phase, calculated as $\rho^{b_{II}} = P_{\text{ambient}}/\mathcal{R}T$ from assumptions); $\mathcal{R} = 8.314$ J·K^{-1}·mol^{-1}, the ideal gas constant; and the pre-exponential factor in Burner II, $k_0^{b_{II}}$, and activation energy $\mathcal{E}^{b_{II}}$ are given by

$$k_0^{b_{II}} = 7.40 \times 10^{11} \text{ mol}^{0.25} \cdot \text{m}^{-0.75} \cdot \text{s}^{-1} \quad \text{and}$$
$$\mathcal{E}^{b_{II}} = 125.5 \text{ kJ} \cdot \text{mol}^{-1}$$

These values are determined experimentally for the temperature range 1,000 K $\leq T \leq$ 2,500 K.

The volume of the burner $V^{b_{II}}$, is the design decision variable. The operational decision variable is the inlet flow rate of butane $F_{C_4H_{10}}^{b_{II}}$.

The total volume of the device V^{tot}, is the sum of the volumes of the burners, reactor and SOFC. Assuming the fixed aspect ratio of a cube, the total area for heat transfer A^{tot}, is a function of the total volume

$$A^{\text{tot}} = 6(V^{\text{tot}})^{2/3}$$

The microfabricated fuel cell stack operates at very high temperatures. The feasibility of microreactor operation at such high temperatures (900°C), where the surrounding packaging temperature does not exceed 50°C, as a result of vacuum packaging has been demonstrated.[22] In this case study, the detailed design of insulation is not considered. Indirectly, insulation affects the choice of coefficients governing the heat transfer to the surroundings.

In the model, the difference between the stack and ambient temperature T_{ambient}, drives the radiative and conductive heat transfer to the ambient. Heat loss is calculated by the formula

$$Q^{\text{loss}} = A^{\text{tot}}(U^{\text{loss}}(T - T_{\text{ambient}}) + \varepsilon\sigma^{\text{SB}}(T^4 - T_{\text{ambient}}^4)) \quad (2)$$

where U^{loss} is the overall heat loss coefficient, and ε is the overall emissivity including the view factor.[13] Heat recovery occurs and effluents at stack temperature are used to preheat the feeds. Heat recovery affects the temperature of the effluents. The effluents leave the stack at the arithmetic average of the ambient and the stack temperature as a result of heat recovery.

The stack temperature T, is an operational decision variable. During usual stack operation, the temperature of the stack is determined once the volumes of the components, fuel-cell operating voltage and influent flow rates are set. By considering T as an operational variable, constraints on the states of Eq. (1) are introduced implicitly via Eq. (2) for each unit operation.

The total heat load $\dot{Q}^{\text{tot}}$, is calculated from the overall heat balance as

$$\dot{Q}^{\text{tot}} = \Delta H - Q^{\text{loss}} - \mathcal{P}^{fc}$$

where ΔH is the difference between the enthalpy flows of the feed and effluent streams, and $\mathcal{P}^{fc}$ is the electrical power

Table 1. Design Decision Variables

Variable	Name	Units
V^{r}	Reactor Volume	m^3
V^{fc}	Fuel-Cell Volume	m^3
$V^{\mathrm{b_I}}$	Burner I Volume	m^3
$V^{\mathrm{b_{II}}}$	Burner II Volume	m^3

produced by the system. To ensure autothermal operation, the total heat load is constrained to zero. Decision variables are adjusted by the optimization to satisfy this constraint.

The operational and design decision variables are summarized in Tables 1 and 2.

Formulation of the Two-Stage Mathematical Program

The amount of fuel expended to produce demand $\mathcal{P}_i$ is defined by the formula

$$\mathcal{F}_i \equiv \mathcal{M}_{\mathrm{NH_3}} F^{\mathrm{r}}_{\mathrm{in},i} + \mathcal{M}_{\mathrm{C_4H_{10}}} F^{\mathrm{b_{II}}}_{\mathrm{C_4H_{10}},i}$$

where $\mathcal{M}_{\mathrm{NH_3}}$ and $\mathcal{M}_{\mathrm{C_4}}\mathrm{H_{10}}$ are the molar masses of NH_3 and C_4H_{10}, respectively.

The objective is to maximize the ratio of total energy produced to the amount of fuel required. Normalizing this ratio by the mission duration, we obtain the *gravimetric mission fuel energy density*

$$\bar{\mathcal{D}}_{\mathrm{m}} \equiv \frac{\sum_{i=1}^{N_d} p_i \mathcal{P}_i}{\sum_{i=1}^{N_d} p_i \mathcal{F}_i}. \tag{3}$$

This objective is appropriate for applications where the mass of the fuel to be carried dominates over the total mass of the power generation equipment, as well as applications where refueling is infrequent due to logistic restrictions. The numerator of Eq. (3) is a constant for given frequencies and values of the power demand. The objective to be minimized for each demand, $\mathcal{P}_i$ is $\mathcal{F}_i$. The objective of (M) is the sum of the optimal solutions of each (L_i) weighted by the frequencies.

The operation at any given power demand is determined by an optimal solution of the program

$$\begin{aligned} \min_{\mathbf{y}} \quad & \mathcal{F}_i(\mathbf{y}) \\ \text{s.t.} \quad & 0 = \mathcal{P}^{fc}(\mathbf{x},\mathbf{y}) - \mathcal{P}_i \end{aligned} \tag{4}$$

$$0 = \dot{\mathcal{Q}}^{\mathrm{tot}}(\mathbf{x},\mathbf{y}) \tag{5}$$

Table 2. Operational Decision Variables

Variable	Name	Units
T	Stack Operation Temperature	K
U	Fuel-Cell Voltage	V
$F^{\mathrm{r}}_{\mathrm{in}}$	Reactor Inlet NH_3 Flow Rate	$\mathrm{mol\cdot s^{-1}}$
$F^{\mathrm{ca}}_{\mathrm{in}}$	Fuel-Cell Cathode Air Inlet Flow Rate	$\mathrm{mol\cdot s^{-1}}$
$F^{\mathrm{b_I}}_{\mathrm{in}}$	Burner I Air Inlet Flow Rate	$\mathrm{mol\cdot s^{-1}}$
$F^{\mathrm{b_{II}}}_{\mathrm{C_4H_{10}}}$	Burner II C_4H_{10} Inlet Flow Rate	$\mathrm{mol\cdot s^{-1}}$

$$0 \geq z^{\mathrm{b_I}}_{\mathrm{NH_3}}(\mathbf{x},\mathbf{y}) - z^{\mathrm{b_I,max}}_{\mathrm{NH_3}} \tag{6}$$

$$0 \geq z^{\mathrm{b_I}}_{\mathrm{NO}}(\mathbf{x},\mathbf{y}) - z^{\mathrm{b_I,max}}_{\mathrm{NO}} \tag{7}$$

$$\mathbf{y} \in Y \tag{8}$$

where the functions $\mathcal{P}^{fc}$, $\dot{\mathcal{Q}}^{\mathrm{tot}}$, $z^{b_I}_{\mathrm{NH_3}}$ and $z^{\mathrm{b_I}}_{\mathrm{NO}}$ compute the power output of the fuel-cell stack, the total heat load, the mole fractions of NH_3 and NO in the effluent of Burner I, respectively, as functions of the design and operational decision variables. Constraint (4) ensures that the fuel stack produces the required power to meet each demand. Constraint (5) ensures autothermal operation. The constraints (6) and (7) limit the mole fractions of NH_3 and NO to acceptable safe levels in the discharge from the stack at each power demand. Box constraints on the operational decision variables are represented by Eq. (8). The functions $\mathcal{P}^{fc}$, $\dot{\mathcal{Q}}^{\mathrm{tot}}$, $z^{\mathrm{b_I}}_{\mathrm{NH_3}}$ and $z^{\mathrm{b_I}}_{\mathrm{NO}}$ are evaluated by numerical integration of the multistage DAEs comprising the model of the micro fuel-cell system.

The final two-stage program is

$$\min_{\mathbf{x}} \quad \sum_{i=1}^{N_d} p_i Q_i \tag{9}$$

$$\left.\begin{aligned} \text{s.t.} \quad & Q_i = \min_{\mathbf{y}} \quad \mathcal{F}_i(\mathbf{y}) \\ & \text{s.t.} \quad 0 = \mathcal{P}^{fc}(\mathbf{x},\mathbf{y}) - \mathcal{P}_i \\ & \qquad 0 = \dot{\mathcal{Q}}^{\mathrm{tot}}(\mathbf{x},\mathbf{y}) \\ & \qquad 0 \geq z^{\mathrm{b_I}}_{\mathrm{NH_3}}(\mathbf{x},\mathbf{y}) - z^{\mathrm{b_{I,max}}}_{\mathrm{NH_3}} \\ & \qquad 0 \geq z^{\mathrm{b_I}}_{\mathrm{NO}}(\mathbf{x},\mathbf{y}) - z^{\mathrm{b_{I,max}}}_{\mathrm{NO}} \\ & \qquad \mathbf{y} \in Y \end{aligned}\right\} \quad \forall i \in \mathcal{J}$$

$$\mathbf{x} \in X \tag{10}$$

where Eq. (10) represents the box constraints shown in Table 3.

For the analysis of the results in the next section, the following additional performance measures are defined. The *mean gravimetric fuel energy density* is

$$\bar{\mathcal{D}} \equiv \sum_{i=1}^{N_d} p_i \mathcal{D}_i \tag{11}$$

and the *gravimetric fuel energy density* $\mathcal{D}_i$, is defined as

Table 3. Bound Constraints for the Decision Variables

Variable	Lower Bound	Upper Bound	Units
V^{r}	0.0	none	m^3
V^{fc}	0.0	none	m^3
$V^{\mathrm{b_I}}$	0.0	none	m^3
$V^{\mathrm{b_{II}}}$	0.0	none	m^3
T	0.0	1100.0	K
U	0.0	1.0	V
$F^{\mathrm{r}}_{\mathrm{in}}$	0.0	none	$\mathrm{mol\cdot s^{-1}}$
$F^{\mathrm{ca}}_{\mathrm{in}}$	0.0	none	$\mathrm{mol\cdot s^{-1}}$
$F^{\mathrm{b_I}}_{\mathrm{in}}$	0.0	none	$\mathrm{mol\cdot s^{-1}}$
$F^{\mathrm{b_{II}}}_{\mathrm{C_4H_{10}}}$	0.0	none	$\mathrm{mol\cdot s^{-1}}$

$$\mathcal{D}_i \equiv \frac{\mathcal{P}_i}{\mathcal{F}_i}. \tag{12}$$

Study results

Two applications for the micro fuel-cell based system are considered. The first application is the design of a system to power the electronic equipment of the dismounted soldier. In this application, the power demand has two possible values: 20.0 W and 50.0 W. The 20.0 W demand occurs 90% of the time.[19] Designs are obtained for 20.0 W demand frequencies of 80.0%, 85.0%, 90.0% and 95.0% to study the effect of varying frequencies. Designs to maximize the mean gravimetric fuel energy density (11) are compared with designs to maximize the mission gravimetric energy density (3), in order to analyze the effect of objective selection and interpretation of the optimization problems. Powering a cellular phone is the second application. The power demands are 0.2 W and 2.0 W corresponding to demands on standby and during a conversation. The cellular phone operates on standby 90% of the time.

Throughout this section, two-stage programming based designs are compared with the results of the following alternative design approaches:

- **Ideal design:** This case represents a design where component volumes can be adjusted optimally for each possible power demand. This design has the best performance, however, it is not realizable.
- **Design for mean power demand:** Disregarding operation at any other demand, the power generation system is designed for the mean power demand, $\mathcal{P}_{\text{mean}}$ given by the formula

$$\mathcal{P}_{\text{mean}} = \sum_{i=1}^{N_d} p_i \mathcal{P}_i.$$

- **Design for mean power demand with an auxiliary battery:** A simple hybrid electrochemical power generation system comprising an ideal auxiliary battery working in tandem with a micro fuel-cell stack is designed. If the actual demand is larger than the mean power demand, the shortfall in power supply is met by the auxiliary battery. If the actual demand is less than the mean power demand, the excess power produced is used to recharge the battery.
- **Conservative design for mean power demand:** This design aims to optimize the performance for the mean power demand during a mission. Unlike the mean power demand design, the design is required to be feasible at all the power demand levels.
- **Design for maximum power demand:** The micro fuel-cell system is designed for the maximum power demand.
- **Design for average power demand:** The mean power demands and the smaller of the power demands are close in value for the applications considered. In addition to the mean power demand design, the micro fuel-cell system is designed for the average of the demands defined by

$$\mathcal{P}_{\text{ave}} = \frac{\sum_{i=1}^{N_d} \mathcal{P}_i}{N_d}.$$

Many more alternative design approaches can be considered. For example, the device can be designed for the mode (most frequently occurring) demand with constraints to ensure feasible operation at other demands. In the applications considered, the mean demand is very close to the mode demand. Therefore, this case is not discussed, as it is almost covered by mean demand designs. Additional comparisons with these designs do not add any more significant insight, and are omitted for the sake of brevity.

All alternative approaches require the solution of an optimization problem to obtain the design and operational parameters. The conservative design for mean power demand is obtained as a solution of the mathematical program

$$\begin{aligned}
\min_{\mathbf{x},\mathbf{y}_{\text{mean}},\mathbf{y}} \quad & \mathcal{M}_{\text{NH}_3} F^{\text{r}}_{\text{in,mean}} + \mathcal{M}_{\text{C}_4\text{H}_{10}} F^{\text{b}_{\text{II}}}_{\text{C}_4\text{H}_{10},\text{mean}} \\
\text{s.t.} \quad & 0 = \mathcal{P}^{fc}(\mathbf{x}, \mathbf{y}_{\text{mean}}) - \mathcal{P}_{\text{mean}} \\
& 0 = \dot{\mathcal{Q}}^{\text{tot}}(\mathbf{x}, \mathbf{y}_{\text{mean}}) \\
& 0 \geq z^{\text{b}_{\text{I}}}_{\text{NH}_3}(\mathbf{x}, \mathbf{y}_{\text{mean}}) - z^{\max}_{\text{NH}_3} \\
& 0 \geq z^{\text{b}_{\text{I}}}_{\text{NO}}(\mathbf{x}, \mathbf{y}_{\text{mean}}) - z^{\text{b}_{\text{I}},\max}_{\text{NO}} \\
& \left.\begin{aligned} 0 &= \mathcal{P}^{fc}(\mathbf{x}, \mathbf{y}_i) - \mathcal{P}_i \\ 0 &= \dot{\mathcal{Q}}^{\text{tot}}(\mathbf{x}, \mathbf{y}_i) \\ 0 &\geq z^{\text{b}_{\text{I}}}_{\text{NH}_3}(\mathbf{x}, \mathbf{y}_i) - z^{\text{b}_{\text{I}},\max}_{\text{NH}_3} \\ 0 &\geq z^{\text{b}_{\text{I}}}_{\text{NO}}(\mathbf{x}, \mathbf{y}_i) - z^{\text{b}_{\text{I}},\max}_{\text{NO}} \end{aligned}\right\} \quad \forall i \in \mathcal{J} \\
& \mathbf{y} \equiv (\mathbf{y}_1, \ldots, \mathbf{y}_{N_d}) \\
& \mathbf{y}_{\text{mean}} \in Y \\
& \mathbf{x} \in X
\end{aligned} \tag{13}$$

where the subscript "mean" denotes values corresponding to the mean power demand. The rest of the alternative design approaches are solutions of mathematical programs of the form

$$\begin{aligned}
\min_{\mathbf{x},\mathbf{y}} \quad & \mathcal{M}_{\text{NH}_3} F^{\text{r}}_{\text{in}} + \mathcal{M}_{\text{C}_4\text{H}_{10}} F^{\text{b}_{\text{II}}}_{\text{C}_4\text{H}_{10}} \\
\text{s.t.} \quad & 0 = \mathcal{P}^{fc}(\mathbf{x}, \mathbf{y}) - \mathcal{P} \\
& 0 = \dot{\mathcal{Q}}^{\text{tot}}(\mathbf{x}, \mathbf{y}) \\
& 0 \geq z^{\text{b}_{\text{I}}}_{\text{NH}_3}(\mathbf{x}, \mathbf{y}) - z^{\text{b}_{\text{I}},\max}_{\text{NH}_3} \\
& 0 \geq z^{\text{b}_{\text{I}}}_{\text{NO}}(\mathbf{x}, \mathbf{y}) - z^{\text{b}_{\text{I}},\max}_{\text{NO}} \\
& \mathbf{y} \in Y \\
& \mathbf{x} \in X,
\end{aligned} \tag{14}$$

with the $\mathcal{P}$ value set to the nominal, the mean, the maximum or the average power demand.

The bound constraints on the decision variables are summarized in Table 3. The upper bound on temperature is set to 1,100.0 K to represent material constraints. The lower bounds on flows and volumes is set to zero and no upper bounds are defined.

The single-level equivalent of Eq. 9 and the programs Eqs. 13,14 are nonlinear nonconvex optimization problems that should be solved to guaranteed global optimality. Methods exist to solve mathematical programs with ordinary differential equations embedded to guaranteed global optimality.[31–33]

However, similar algorithms for mathematical programs with multistage DAEs embedded are not available at present.

In this article, a local nonlinear optimization algorithm (SQP) coupled with a multistart procedure is employed to determine the optimal solutions. For all alternative design formulations, only two local minima are identified as a result of multistart procedures. One local minimum corresponds to the case where half of the residual ammonia is converted to nitric oxide at the end of the Ammonia line, the other local minimum corresponds to the case where all the ammonia is converted to nitric oxide. It is observed that the optimal solution value corresponding to the second case is less than the solution value corresponding to the first case. The solution for the second case is taken as the global solution similar to prior work.[15] All local minima obtained as the solution of the single-level equivalent formulations exhibit total conversion of ammonia into nitric oxide for all power demands. The best solution of the local minima obtained from the multistart procedure is taken as the global solution of the single-level equivalent formulations.

SNOPT[34] is used as the SQP solver. For consistent initialization and integration of the multistage DAEs, subroutines from DAEPACK[35] are employed. The subroutine DSL48S[36–38] is used to integrate the equations numerically, and obtain the first-order sensitivities required to calculate gradient information for the SQP solver. The subroutine BLOCKSOLVE[39] is used for consistent initialization of DAEs. The necessary differentiations of the model equations with respect to the decision variables for consistent initialization and calculation of sensitivities are obtained using DAEPACK's automatic differentiation features. The relative and absolute tolerances for integration of the DAEs are 1×10^{-7} and 1×10^{-8}, respectively. The tolerances used in the SQP solver are taken two order of magnitudes larger than the integration tolerances. Even though the numerical results are obtained using such tight tolerances, results are only reported to three significant digits due to the inherent inaccuracy of the model.

Since the multistart approach does not guarantee global optimality, there is a possibility that the global minimum is not obtained, and the best solution is only a local minimum of the single-level equivalent of the two-stage program. Nevertheless, a local minimum solution of the single-level equivalent is still an optimal design in the sense that for small perturbations of the solution, one cannot obtain a better design. Furthermore, a local solution still satisfies the power, bound and discharge constraints. Additional discussion on this topic can be found in the appendix.

The results are arranged in four sections. First, the performance of a nominal power demand design at differing power demands is presented. Second, the performance of the two-stage programming based design is compared with alternative designs. Third, the difference in design due the interpretation of the optimization problems is demonstrated. Last, the influence of frequencies on the performance and design are presented.

Nominal power demand design performance. The performance of a nominal power demand design in case of varying power demand is investigated. A similar study has been published.[16] The ideal operational and design decision variables for a particular demand are obtained as a solution of

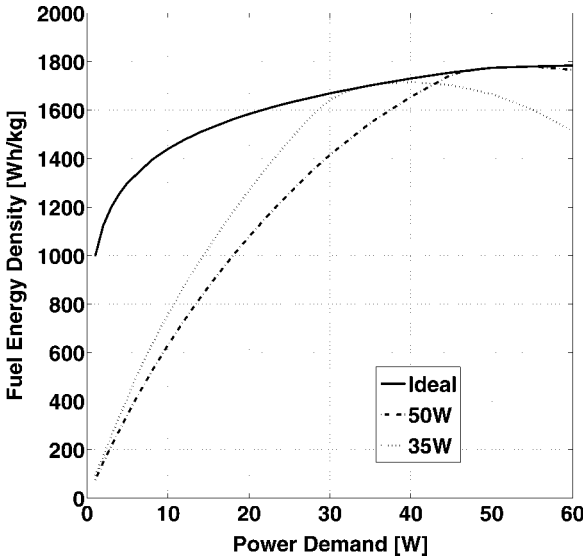

Figure 2. Performance of fuel-cell stack designs for 35.0 W and 50.0 W in case of varying power demands.

(14) with $\mathcal{P}$ set to the particular demand. The gravimetric fuel energy density (12) is calculated using the ideal design decision variables. The curve with the label "ideal" in Figure 2 is obtained using gravimetric fuel energy densities calculated in the described manner for demands up to 60.0 W. The ideal curve shows the highest fuel energy density attainable for a given power demand. The ideal fuel energy density curve varies with power demand more drastically for smaller power demands mainly due to heat loss effects.[13,14]

In order to obtain the curve with the label "50 W", the optimal unit operation volumes obtained for a nominal power demand of 50.0 W are used. Then, the optimization problem (14) is solved for demands up to 60.0 W to determine the operational design decision variables by setting the unit operation volumes to the 50.0 W nominal demand design values. The fuel energy densities are calculated using these operational decision variable values. The solutions represent the optimal operational variables to produce a particular demand given a device designed for 50.0 W demand. As expected, the ideal and the 50.0 W curve intersect at 50.0 W demand. The curve labeled "35 W" is obtained in the same manner as the "50 W" curve with the nominal power demand set to 35.0 W.

The performances of the 50.0 W and 35.0 W demand designs over the power demand range of interest vary significantly. Performance degrades to unacceptable levels when the actual demand and the design demand differ significantly. In the dismounted soldier application, any nominal power demand design suffers this degradation as can be seen from the 35.0 W and 50.0 W curves. The significant degradation in performance of a nominal power demand design when the actual demand is far from the nominal one motivates the search for other methods to determine design and operational decision variables for applications with varying power demand.

The curve for 20.0 W nominal demand design is not plotted as it does not result in feasible operation over the whole range of power demands. This is the result of the interaction between heat losses, chemical flow rates, unit operation vol-

umes and constraints on the operation. In case the actual demand is less than the design demand, the total volume of the micro fuel-cell system is larger than the volume of the optimal design for that demand. More heat losses occur than is ideal during operation to meet the actual demand. Larger amounts of butane than ideally required are used to keep the stack at a constant operating temperature, decreasing the performance. In case the actual demand is higher than the nominal demand, the volumes are smaller than the optimal volumes for that demand. Smaller volumes lead to lower conversions in the reactor and fuel-cell. Lower conversion necessitates higher flow rates of ammonia to provide the necessary H_2 to meet the power demand. Mole fractions of NH_3 and NO in the effluent increase as higher flow rates and smaller volumes result in lower residence times in the units. Larger airflow rates are required to dilute the mole fraction of NH_3 and NO to acceptable and safe levels. Even though heat losses decrease, more C_4H_{10} is required in order to heat up this air. The efficiency of the butane burner decreases with increased C_4H_{10} flow rate due to shorter residence times, and eventually a demand is reached for which the constraints on the NH_3 and NO mole fractions cannot be met by increasing the airflow rates while operating autothermally. As a result, it is not feasible to produce 50.0 W with a 20.0 W nominal power demand design.

Comparison of design performances. In this section, the performance of various other designs are compared to the design obtained as a result of the proposed two-stage optimization method. The comparisons involve micro fuel-cell systems intended to power the dismounted soldier and micro fuel-cell systems for cellular phone applications.

The *ideal gravimetric mission fuel energy density* is calculated as

$$\bar{\mathcal{D}}_{\mathrm{m}}^{\mathrm{ideal}} = \frac{\sum_{i=1}^{N_d} p_i \mathcal{P}_i}{\sum_{i=1}^{N_d} p_i \mathcal{F}_i^{\mathrm{ideal}}}$$

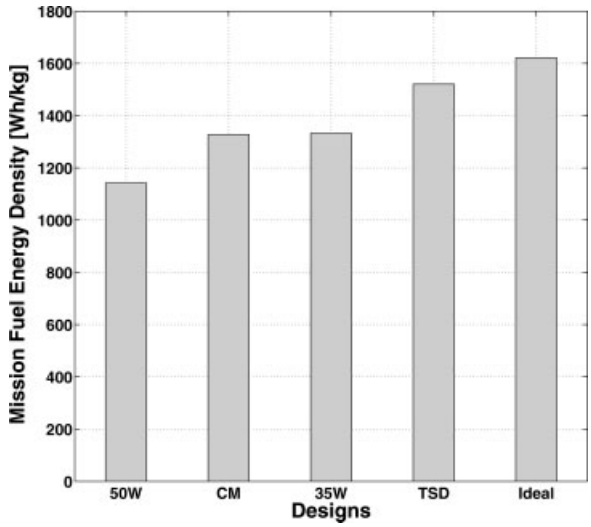

Figure 3. Comparison of various design strategies for the dismounted soldier application.

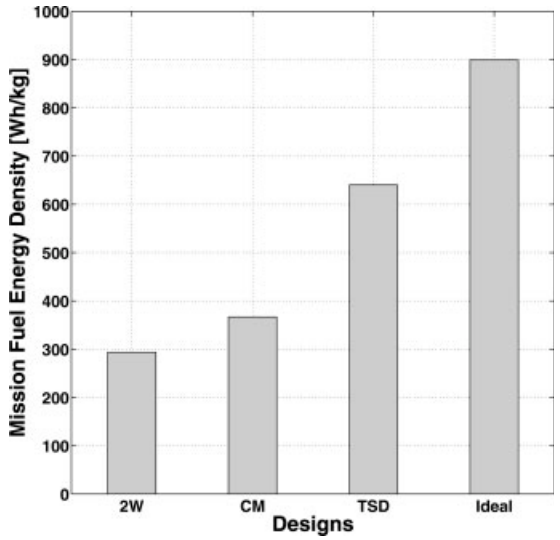

Figure 4. Comparison of various design strategies for the cellular phone application.

where $\mathcal{F}_i^{\mathrm{ideal}}$ represent the ideal fuel expenditure for each $\mathcal{P}_i$ obtained from the ideal design for $\mathcal{P}_i$ nominal power demand design. The *gravimetric mission fuel energy density based on mean power demand design* is defined by the formula

$$\bar{\mathcal{D}}_{\mathrm{m}}^{\mathrm{mean}} \equiv \frac{\sum_{i=1}^{N_d} p_i \mathcal{P}_i}{\sum_{i=1}^{N_d} p_i \mathcal{F}_i^{\mathrm{mean}}}$$

where $\mathcal{F}_i^{\mathrm{mean}}$ represent the fuel expenditure to produce each $\mathcal{P}_i$ with a system designed for the mean power demand. Similar formulae are applied to obtain performances for any other nominal power demand design with appropriate fuel expenditure values.

In Figures 3 and 4, *TSD*, represents the performance of the design obtained using the proposed method. *Ideal* represents the performance of the ideal design, and *CM* represents the conservative design for mean power demand. Performances of nominal power demand based designs are labeled by the nominal power demand value. In both the dismounted soldier and cellular phone applications, the design based on mean power demand results in infeasible operation at the higher power demand value. Autothermal operation cannot be maintained due to the reasons discussed in the previous section. Hence, $\bar{\mathcal{D}}_{\mathrm{m}}^{\mathrm{mean}}$ for both applications is ∞.

The difference between $\bar{\mathcal{D}}_{\mathrm{m}}^{\mathrm{ideal}}$ and TSD values for the dismounted soldier application is only 100 W·h·kg^{-1} (Figure 3). The proposed method recovers a significant portion of the best theoretical possible performance. The two-stage programming based design results in 25% lower fuel expenditure than the maximum power demand (50.0 W) design, and 13% lower fuel expenditure than either the conservative mean power demand or the average power demand (35.0 W) design. In the cellular phone design case (Figure 4), the difference between $\bar{\mathcal{D}}_{\mathrm{m}}^{\mathrm{ideal}}$ and TSD value is 260 W·h·kg^{-1}. The

Table 4. Comparison of Fuel Energy Densities for Designs employing a Battery and the Two-Stage Programming based Design for the Dismounted Soldier Case

Design	$\bar{\mathcal{D}}_{\mathrm{m}}^{\mathrm{eq}}$ [W·h·kg^{-1}]	$\mathcal{D}^{\mathrm{eq}}$ [W·h·kg^{-1}]	
		20.0 W	50.0 W
TSD	1520	1500	1590
Auxiliary battery, 700 W·h·kg^{-1}	1270	1610	950
Auxiliary battery, 300 W·h·kg^{-1}	990	1610	480

Table 5. Comparison of Fuel Energy Densities for Designs employing a Battery and the Two-Stage Programming based Design for the Cellular Phone Application

Design	$\bar{\mathcal{D}}_{\mathrm{m}}^{\mathrm{eq}}$ [W·h·kg^{-1}]	$\mathcal{D}^{\mathrm{eq}}$ [W·h·kg^{-1}]	
		0.2 W	2.0 W
TSD	640	460	1000
Auxiliary battery, 700 W·h·kg^{-1}	560	840	720
Auxiliary battery, 300 W·h·kg^{-1}	380	840	340

two-stage programming based design reduces fuel expenditure by more than 50% with respect to fuel the maximum power demand design (2 W), and by 40% with respect to the conservative mean power demand design. The design for average power is also infeasible for the cellular phone application. The reduction in fuel expenditure due to the proposed methodology at lower power demands is significantly better than at higher power demands. This is a direct result of the fuel energy density varying more rapidly with demand at lower power demands.

The mean power demand based design cannot operate feasibly to meet the maximum power demand in both the soldier and the cellular phone applications. An auxiliary battery can be used in tandem to make the mean power demand design feasible for all power demands. In this hybrid electrochemical approach, the required mass of the battery is important. The mass of the battery is treated similar to the mass of fuel as it is dependent on the power demand and the mission duration.

To facilitate comparison, the *equivalent fuel expenditure* is defined by the formula

$$\mathcal{F}_i^{\mathrm{eq}} \equiv \mathcal{F}_{\mathrm{mean}} + \frac{\max\{\mathcal{P}_i - \mathcal{P}_{\mathrm{mean}}, 0\}}{\mathcal{D}_{\mathrm{battery}}} \tag{15}$$

where $\mathcal{D}_{\mathrm{battery}}$ represents the gravimetric fuel energy density of the battery and

$$\mathcal{F}_{\mathrm{mean}} \equiv \mathcal{M}_{\mathrm{NH_3}} F^{\mathrm{r}}_{\mathrm{in,mean}} + \mathcal{M}_{\mathrm{C_4H_{10}}} F^{\mathrm{b_{II}}}_{\mathrm{C_4H_{10},mean}}.$$

The ratio $(\mathcal{P}_i - \mathcal{P}_{\mathrm{mean}})/\mathcal{D}_{\mathrm{battery}}$ represents the mass of battery required in unit time to meet the difference in power demand and power supplied by the fuel-cell system. The equivalent fuel expenditure (15) penalizes the usage of the battery in case the fuel-cell system cannot meet the demand ($\mathcal{P}_i - \mathcal{P}_{\mathrm{mean}} > 0$). Otherwise battery usage is not penalized. If the output of the fuel-cell stack meets or exceeds the demand, the fuel consumption is not reduced and the excess energy produced is stored in the battery. It is assumed that energy storage in the battery, as well as retrieval from the battery occurs without any losses. As a result, the energy stored in the battery and the energy retrieved from the battery during a mission are equal for a mean power demand design. This ideal case represents an upper bound on the performance of the hybrid electrochemical system containing a fuel-cell and an auxiliary battery.

The *equivalent gravimetric fuel energy density* is

$$\mathcal{D}_i^{\mathrm{eq}} \equiv \frac{\mathcal{P}_i}{\mathcal{F}_i^{\mathrm{eq}}}.$$

The *equivalent gravimetric mission fuel energy density* is defined as

$$\bar{\mathcal{D}}_{\mathrm{m}}^{\mathrm{eq}} \equiv \frac{\sum_{i=1}^{N_d} p_i \mathcal{P}_i}{\sum_{i=1}^{N_d} p_i \mathcal{F}_i^{\mathrm{eq}}}.$$

For the following comparisons, two rechargeable batteries with the gravimetric fuel energy densities of 300 W·h·kg^{-1} and 700 W·h·kg^{-1} are considered.[1,2] These values represent highly optimistic performances for batteries. For the purpose of this article, these values help establish an optimistic upper bound on the performance of a mean power demand design with an auxiliary battery with which to compare the proposed two-stage programming based design approach.

Tables 4 and 5 summarize the performance of the designs. When the mean demand is greater than the actual demand, the mass of the battery does not affect the equivalent fuel expenditure (15), and the equivalent gravimetric fuel energy density. Hence, for the dismounted soldier case, the equivalent gravimetric fuel energy density is the same irrespective of battery type when the demand is 20.0 W. It is equal to the gravimetric fuel energy density of the micro fuel-cell system designed for the mean power demand and operating to meet the mean power demand. The same situation occurs in the cellular phone application for the 0.2 W demand. For the cellular phone design case, one can use a battery with an energy density of 700 W·h·kg^{-1} only to achieve better mission fuel energy density. In all other cases, the design based on two-stage mathematical programming outperforms the mean power demand design with an auxiliary battery.

Effect of formulation interpretation on design. The designs for maximizing the mission energy density (3), and

Table 6. Comparison of Fuel Energy Densities for Different Objective Functions

Objective	$\bar{\mathcal{D}}_{\mathrm{m}}$ [W·h·kg^{-1}]	$\bar{\mathcal{D}}$ [W·h·kg^{-1}]	$\mathcal{D}$ [W·h·kg^{-1}]	
			20.0 W	50.0 W
$\max\{\bar{\mathcal{D}}_{\mathrm{m}}\}$	1520	1510	1500	1590
$\max\{\bar{\mathcal{D}}\}$	1470	1520	1560	1240

Table 7. Comparison of Design and Operational Variables for Different Objective Functions

		F_{in}^{r} [μmol·s^{-1}]		F_{in}^{ca} [μmol·s^{-1}]		$F_{in}^{b_I}$ [μmol·s^{-1}]		$F_{C_4H_{10}}^{b_{II}}$ [μmol·s^{-1}]	
Objective	V^{tot} [mm^3]	20.0 W	50.0 W	20.0 W	50.0 W	20.0 W	50.0 W	20.0 W	50.0 W
$\max\{\bar{\mathcal{D}}_m\}$	1.62×10^4	136	500	638	2500	0	0	23.8	3.91
$\max\{\bar{\mathcal{D}}\}$	1.22×10^4	135	661	623	4950	0	0	22.0	0

maximizing the mean energy density (11), are compared for the dismounted soldier application. The mean or expected value of a quantity is the objective used in stochastic programming with recourse. The goal is to optimize the expected performance of the micropower generation system over a large number of missions assuming that power demand is a random variable.

Performance and decision variables are compared in Tables 6 and 7, respectively. The mean energy density maximizing design is obtained by solving Eq. (9) with the objective replaced with the maximization of Eq. (11). Even though the performances measured as fuel energy densities are close, the designs are significantly different. Maximizing mission energy density results in a design with 30% larger volume (7). Unit efficiencies are higher and smaller quantities of ammonia are required. The fuel energy density at the 50.0 W power demand is better in case the mission fuel energy density is maximized. The larger volume results in more heat losses and larger quantities of butane are required for autothermal operation. In case mean energy density is maximized, more air is required at higher demand operation to cool down the stack since the smaller surface area limits heat dissipation. No butane is required to operate the mean fuel energy density maximizing design at steady-state to produce 50.0 W; however, butane is still required to start up power generation and heat the stack to the steady-state operating temperature. Less fuel needs to be transported for the device maximizing mission fuel energy density. This design favors performance at higher demands significantly more. For applications where the mass of the fuel dominates the power generation system mass, the maximization of gravimetric mission energy density is the correct choice.

Effect of frequencies on design. The effect of variations in frequency of occurrence on the design and steady-state operation are investigated for the dismounted soldier application by varying the frequency of the 20.0 W demand from 80% to 95%. The micro fuel-cell stack is designed to maximize the mission gravimetric energy density.

In the figures containing comparison data, solid lines represent the values for a 50.0 W nominal power demand design and dashed lines represent the values for a 20.0 W nominal power demand design. When data is presented for each possible power demand separately, the correspondence between power demand and values is displayed by the legend of the figure. The data is obtained by solving (9) for 20.0 W demand frequencies of 80.0%, 85.0%, 90.0% and 95.0%.

The reactor volume increases with increasing 20.0 W demand frequency (Figure 5). The increase is necessary to maintain acceptable fractional conversion of NH_3 in face of higher flow rates in order to produce 50.0 W and simultaneously meet the discharge constraints. At very high-frequencies, the reactor volume is larger than the ideal reactor volume of a 50.0 W design for this reason. The SOFC volumes are larger than the 20.0 W nominal demand design, but significantly less than the 50.0 W nominal demand design (Figure 6).

The volume of the reactor and SOFC directly affect the extent to which H_2 is produced and oxidized. Since the SOFC volume is significantly less than the 50.0 W nominal power design, a significantly larger NH_3 flow rate is required to produce 50.0 W (Figure 7). On the other hand, a slightly smaller NH_3 flow rate is required to produce 20.0 W since the larger SOFC volumes results in higher SOFC efficiencies at this demand. Larger unit volumes result in larger heat losses. This necessitates the combustion of more C_4H_{10} to maintain a a steady operating temperature at 20.0 W compared to ideal operation at 20.0 W demand (Figure 8). Smaller C_4H_{10} flow rates are required for autothermal operation to produce 50.0 W. At 50.0 W operation, a significant amount of the heat produced by butane combustion is used to warm the air. More air is required to meet the discharge constraints (Figure 9).

The optimal stack operating temperature is always 1,100 K to produce 50.0 W. The micro fuel-cell operates more efficiently at higher-temperatures.[15] The optimal stack temperature to produce 20.0 W is less than 1,100 K in order to reduce the additional heat losses incurred by larger volumes (Figure 10). As the total volume decreases, the stack temperature for 20.0 W demand approaches 1,100 K. In comparison, both the 20.0 W and 50.0 W nominal demand designs operate at 1,100 K.

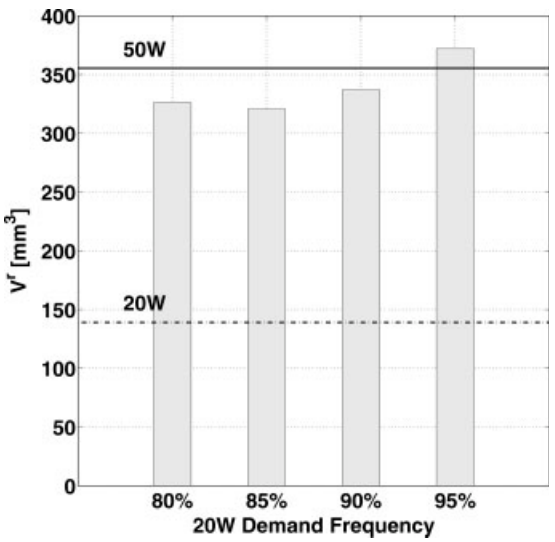

Figure 5. Effect of demand frequency on reactor volume for the dismounted soldier application.

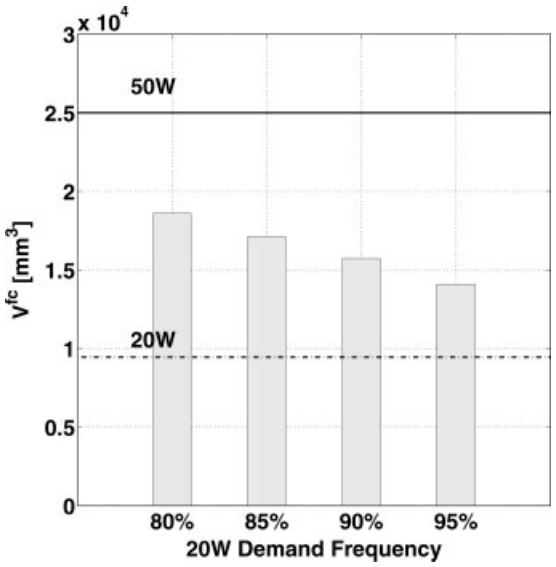

Figure 6. Effect of demand frequency on SOFC volume for the dismounted soldier application.

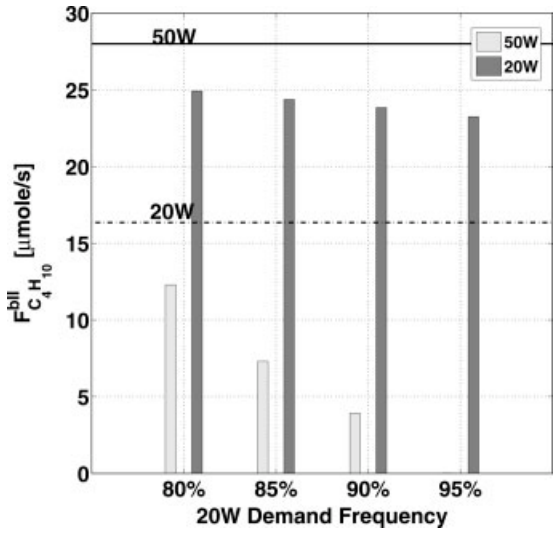

Figure 8. Effect of demand frequency on burner II C_4H_{10} inlet flow rate for the dismounted soldier application.

The fuel energy densities attained for each separate power demand are shown in Figure 11. A trend that favors 20.0 W demand performance as the 20.0 W demand frequency increases is observable. Over the range of frequencies, the performance of operation at both power demands remains very high.

As the frequency of 20.0 W demand approaches 100%, the optimal design and operational decision variables do not converge to the 20.0 W nominal demand optimal design values. The values approach values of a design for 20.0 W nominal demand with additional constraints to ensure feasible operation at other demands. In the limit, the volumes remain larger. The performance to produce 20.0 W does not converge to the 20.0 W nominal power demand design performance and performance to produce 50.0 W deteriorates rapidly as the penalty on the fuel expenditure to produce 50.0 W becomes insignificant.

In Figure 12, the loss of performance in case the actual frequency of 20.0 W demand is different from the design frequency is plotted. A design is obtained for the dismounted soldier application using the proposed method and assuming that 20.0 W demand occurs 90% of the time during a mission. The lighter colored bar graph shows the performance of this design in case the demand frequency is not the same as the design frequency. The darker area in the bar graph show the difference between the performance of this design and

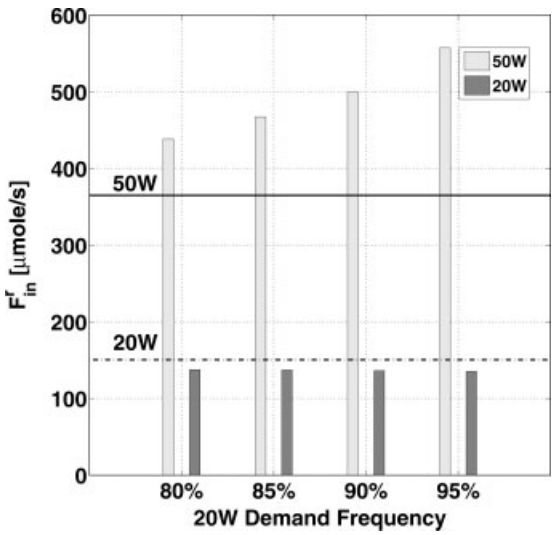

Figure 7. Effect of demand frequency on reactor inlet NH_3 flow rate for the dismounted soldier application.

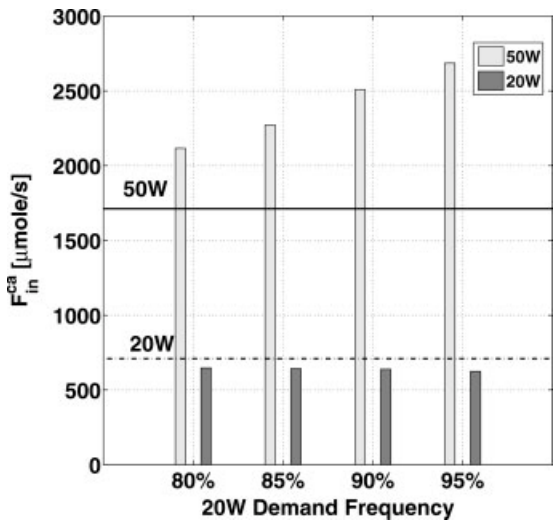

Figure 9. Effect of demand frequency on fuel cell cathode air inlet flow rate for the dismounted soldier application.

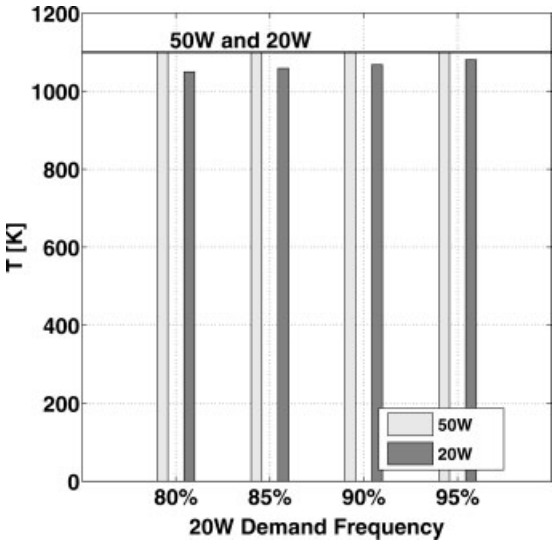

Figure 10. Effect of demand frequency on stack temperature for the dismounted soldier application.

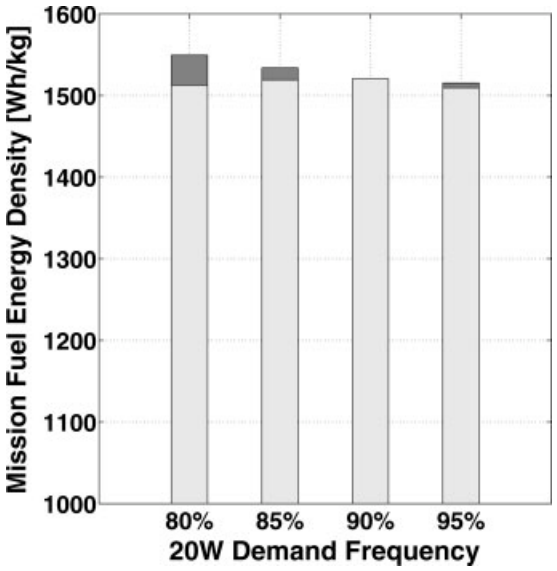

Figure 12. Variation in performance for various frequencies of 20.0 W demand occurrence.

what can be obtained from a design based on the proposed method using the actual frequency. Overall, the difference (loss) of performance is less than 5%, and as expected the loss in performance increases with increasing discrepancy.

Conclusions and Future Work

In this study, a mathematical programming approach is proposed to determine the optimal design and operational parameters of a micropower generation system operating under varying power demands. The steady-state power demand is considered. The varying power demand is represented as a collection of demands occurring at certain frequencies during operation. Constraints on the operation of the device for each power demand are transcribed into a mathematical program. This set of mathematical programs is incorporated as constraints into a top level mathematical program encoding power demand independent constraints to obtain a two-stage formulation. An equivalent single-level formulation for calculation of numerical solutions is presented. The relationship with two-stage stochastic recourse problems is discussed.

The design of a micro fuel-cell stack using ammonia and butane is considered as a case study. An intermediate-fidelity model of the proposed process is incorporated into the two-stage mathematical program. The optimal volumes of the reaction chambers and the fuel flow rates are determined. The two-stage programming based designs obtained are compared with other designs based on nominal power demands. The effect of variations in the frequencies on the optimal design is studied.

The solutions to the two-stage programs are obtained using nonlinear programming solvers and multistart procedures. Even though the location of a global optimal solution cannot be guaranteed by this technique, the case study clearly demonstrates the existence of significantly better designs as a result of incorporating more information about demand variability in the decision process. In all cases considered, significantly better system performance and/or designs with significantly smaller volumes are obtained, justifying the effort to solve computationally difficult optimization problems resulting from two-stage formulations.

This article focuses only on the variations in the power demand at steady-state operation. The fuel cost of switching from one power output level to the next is not considered. Furthermore, the demand model is insensitive to temporal effects, such as the frequency of switchings. This study can be extended to incorporate temporal and switching effects. The framework can also be employed to quantify the temporal effects of demand variability. One direction is to redefine the power demands as functionals representing demand pro-

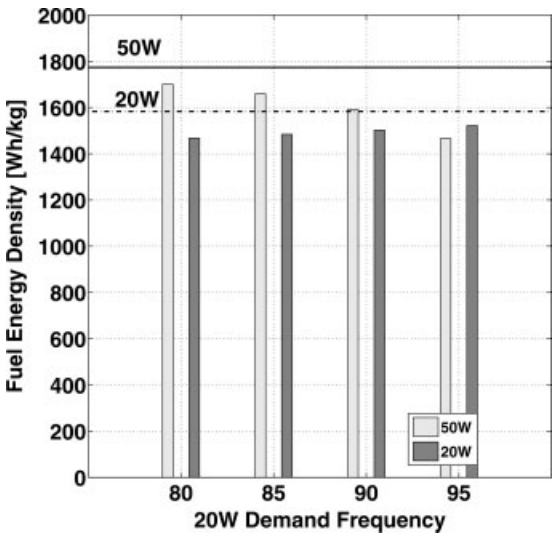

Figure 11. Variation in fuel energy densities for various frequencies of 20.0 W demand occurrence for the dismounted soldier application.

files over a mission duration. Dynamic optimization can be employed to determine corresponding optimal design parameters and time profiles of the operational parameters.

Another direction of future work is the modeling of micropower generation systems with multiple power sources operating in tandem, such as batteries, capacitors and multiple fuel cells, as well as the additional hardware required to interface the systems to portable electronic devices. This effort is motivated by the fact that fuel cell based systems are slow to respond to fast demand changes, and the best design may incorporate more than one power source to compensate for the slow response times of fuel cell based systems. In this regard, the mean power demand design with an auxiliary battery constitutes a starting point for transient performance analysis. The battery is intended to meet a sudden surge in demand. The fuel-cell produces power to keep the battery charged. Even in this case, the fuel-cell stack could operate at some arbitrary nominal power output level. The choice of output level can be made using mathematical programming. Instead of keeping the power output of the fuel-cell stack constant during the whole mission, it can be adjusted at each power demand level. The required battery mass can be incorporated into the proposed two-stage mathematical programming design method by introducing another design decision variable representing the mass of the battery.

Notation

A^{tot} = overall heat transfer surface area, m^2

$\bar{\mathcal{D}}$ = mean gravimetric fuel energy density, $W{\cdot}h{\cdot}kg^{-1}$

$\bar{\mathcal{D}}_{\text{m}}$ = gravimetric mission fuel energy density, $W{\cdot}h{\cdot}kg^{-1}$

$\bar{\mathcal{D}}_{\text{m}}^{\text{eq}}$ = equivalent gravimetric mission fuel energy density, $W{\cdot}h{\cdot}kg^{-1}$

$\bar{\mathcal{D}}_{\text{m}}^{\text{ideal}}$ = ideal gravimetric mission fuel energy density, $W{\cdot}h{\cdot}kg^{-1}$

$\bar{\mathcal{D}}_{\text{m}}^{\text{mean}}$ = gravimetric mission fuel energy density, based on mean power demand design, $W{\cdot}h{\cdot}kg^{-1}$

$\mathcal{D}$ = gravimetric fuel energy density, $W{\cdot}h{\cdot}kg^{-1}$

$\mathcal{D}^{\text{eq}}$ = equivalent gravimetric fuel energy density, $W{\cdot}h{\cdot}kg^{-1}$

$\mathcal{E}^{\text{b}_{\text{II}}}$ = activation energy, $kJ{\cdot}mol^{-1}$

$\mathcal{F}$ = fuel expenditure, $kg{\cdot}s^{-1}$

$\mathcal{F}^{\text{eq}}$ = equivalent fuel expenditure, $kg{\cdot}s^{-1}$

F = molar flux, $mol{\cdot}s^{-1}$

$F_{\text{C}_4\text{H}_{10}}^{\text{b}_{\text{II}}}$ = Burner II C_4H_{10} inlet flow rate, $mol{\cdot}s^{-1}$

$F_{\text{in}}^{\text{b}_{\text{I}}}$ = Burner I air inlet flow rate, $mol{\cdot}s^{-1}$

$F_{\text{in}}^{\text{ca}}$ = fuel-cell cathode air inlet flow rate, $mol{\cdot}s^{-1}$

F_{in}^{r} = reactor inlet NH_3 flow rate, $mol{\cdot}s^{-1}$

ΔH = difference between influent and effluent enthalpy streams, W

$\mathcal{I}_c$ = set of chemicals in the microfuel-cell stack {NH_3, C_4H_{10}, N_2, H_2O, O_2, NO, CO_2}

$k_0^{\text{b}_{\text{II}}}$ = pre-exponential factor, $mol^{0.25}{\cdot}m^{-0.75}{\cdot}s^{-1}$

$\mathcal{M}_{\text{NH}_3}$ = molar mass of NH_3, $kg{\cdot}mol^{-1}$

$\mathcal{M}_{\text{C}_4\text{H}_{10}}$ = molar mass of C_4H_{10}, $kg{\cdot}mol^{-1}$

N_d = Number of possible power demands

$\mathcal{P}$ = power demand, W

$\mathcal{P}^{\text{fc}}$ = fuel-cell power output, W

$\mathcal{P}_i$ = possible values for power demand $\mathcal{P}$, W

$\mathcal{P}_{\text{ave}}$ = average power demand, W

$\mathcal{P}_{\text{mean}}$ = mean power demand, W

P_{ambient} = ambient pressure, Pa

$\mathcal{Q}^{\text{tot}}$ = total heat load, W

$\mathcal{R}$ = ideal gas constant, $J{\cdot}K^{-1}{\cdot}mol^{-1}$

r = reaction rate, various units

$r^{\text{b}_{\text{II}}}$ = reaction rate in Burner II, $mol{\cdot}m^{-3}{\cdot}s^{-1}$

T = microfuel-cell stack operation temperature, K

T_{ambient} = ambient temperature, K

U = fuel-cell voltage, V

U^{loss} = overall heat loss coefficient, $W{\cdot}m^{-2}{\cdot}K^{-1}$

V = volume, m^3

$V^{\text{b}_{\text{II}}}$ = burner II volume, m^3

$V^{\text{b}_{\text{I}}}$ = burner I volume, m^3

V^{fc} = fuel-cell volume, m^3

V^{r} = reactor volume, m^3

V^{tot} = total volume of the burners, fuel-cell and the reactor, m^3

z = mole fraction, dimensionless

$z_{\text{C}_4\text{H}_{10}}^{\text{b}_{\text{II}}}$ = molar fraction of C_4H_{10} in Burner II, dimensionless

$z_{\text{O}_2}^{\text{b}_{\text{II}}}$ = molar fraction of O_2 in Burner II, dimensionless

$z_{\text{NH}_3}^{\text{b}_{\text{I}},\text{max}}$ = maximum allowable NH_3 mole fraction in burner I effluent, dimensionless

$z_{\text{NO}}^{\text{b}_{\text{I}},\text{max}}$ = maximum allowable NO mole fraction in burner I effluent, dimensionless

$z_{\text{NH}_3}^{\text{b}_{\text{I}}}$ = molar fraction of NH_3 in the burner I effluent, dimensionless

$z_{\text{NO}}^{\text{b}_{\text{I}}}$ = molar fraction of NO in the burner I effluent, dimensionless

Acronyms

DAE = differential algebraic equation

PFR = plug flow reactor

SQP = successive quadratic programming

SOFC = solid oxide fuel-cell

Greek letters

ε = product of emissivity and view factor, dimensionless

η = scaled axial coordinate, dimensionless

ν = stoichiometric coefficient, dimensionless

ρbII = total molar density in burner II, $mol{\cdot}m^{-3}$

σSB = Stefan-Boltzmann constant, $W{\cdot}m^{-2}{\cdot}K^4$

Acknowledgments

Financial support was provided by the DoD Multidisciplinary University Research Initiative (MURI) program administered by the Army Research Office under Grant DAAD19-01-1-0566.

Literature Cited

1. Linden D. *Handbook of Batteries*. New York: McGraw-Hill; 2001.
2. Brodd JR. Recent developments in batteries for portable consumer applications. *Electrochem Soc Interf*. 1999;8:20–23.
3. Dyer CK. Fuel cells for portable applications. *J Power Sources*. 2002;106:31–34.
4. Epstein AH, Senturia SD. Macro power from micro machinery. *Science*. 1997;276:1211.
5. Coutts TJ. A review of progress in thermophotovoltaic generation of electricity. *Renew Sust En Rev*. 1999;3:77–184.
6. Dyer CK. Replacing the battery in portable electronics. *Scientific American*. 1999;281:88–93.
7. Jensen KF. Microreaction engineering-is small better? *Chem Eng Sci*. 2001;56:293–303.
8. Haile SM. Fuel-cell materials and components. *ACTA Materialia*. 2003;51:5981–6000.
9. Shao ZP, Haile SM, Ahn J, Ronney PD, Zhan ZL, Barnett SA. A thermally self-sustained micro solid-oxide fuel-cell stack with high power density. *Nature*. 2005;435:795–798.
10. Desmukh SR, Mhadeshwar AB, Vlachos DG. Microreactor modeling for hydrogen production from ammonia decomposition on ruthenium. *Ind and Eng Chem Res*. 2004;43:2986–2999.
11. Srikar VT, Turner KT, Ie TYA, Spearing SM. Structural design considerations for micromachined solid-oxide fuel-cell. *J Power Sources*. 2004;125:186–200.
12. Pattekar AV, Kothare MV. A microreactor for hydrogen production in micro fuel-cell applications. *IEEE J of Microelectromechanical Systems*. 2004;13:7–18.
13. Mitsos A, Palou-Rivera I, Barton PI. Alternatives for micropower generation processes. *Ind and Eng Chem Res*. 2004;43:74–84.
14. Mitsos A, Henke MM, Barton PI. Product engineering for man-portable power generation based on fuel cells. *AIChE J*. 2005;51:2199–2219.

15. Chachuat B, Mitsos A, Barton PI. Optimal design and steady-state operation of micro power generation employing fuel cells. *Chem Eng Sci*. 2005;60:4535–4556.
16. Barton PI, Mitsos A, Chachuat B. Optimal start-up of micro power generation processes. In: Puigjaner C. ed. *European Symposium on Computer Aided Process Engineering - 15*: Elsevier; 2005;1093–1098.
17. Chachuat B, Mitsos A, Barton PI. Optimal start-up of microfabricated power generation processes employing fuel cells. In preparation.
18. Mahesri A, Vardhan V. Power Consumption Breakdown on a Modern Laptop. Workshop on Power Aware Computing Systems, 37th International Symposium on Microarchitecture December; 2004.
19. Soldier Power/Energy Systems Committee. *Meeting the Energy Needs of Future Warriors*. Washington DC: The National Academies Press; 2004.
20. Birge JR, Louveaux F. *Introduction to Stochastic Programming*. Springer Series in Operations Research, New York: Springer-Verlag; 1997.
21. Kall P, Wallace SW. *Stochastic Programming*. New York: John Wiley & Sons; 1995.
22. Arana LR, Schaevitz SB, Franz AJ, Martin AS, Jensen KJ. A microfabricated suspended-tube chemical reactor for thermally efficient fuel processing. *J of Microelectromechanical Systems*. 2003;12(5): 600–612.
23. Ganley JC, Seebauer EG, Masel RI. Porous anodic alumina microreactors for production of hydrogen from ammonia. *AIChE J*. 2004;50:829–834.
24. Sifer N, Gardner K. An analysis of hydrogen production from ammonia hydride hydrogen generators for use in military fuel-cell environments. *J of Power Sources*. 2004;132:135–138.
25. Mitsos A, Chachuat B, Barton PI.Justification of the modeling assumptions in the intermediate fidelity models for portable power generation. Technical report. Cambridge (MA): Massachusetts Institute of Technology, Process Systems Engineering Laboratory; 2005. (Available at: http://yoric.mit.edu/reports.html).
26. Fogler HS. *Elements of Chemical Reaction Engineering*. Englewood Cliffs, NJ: Prentice-Hall; 1998.
27. Barton PI, Lee CK. Modeling, simulation, sensitivity analysis and optimization of hybrid systems. *ACM Trans on Model and Comp Sim*. 2002;12:256–289.
28. Safety and Health Topics: Ammonia. Washington DC: Occupational Safety & Health Administration. (Available at: http://www.osha.gov/dts/chemicalsampling/data/CH_218300.html).
29. Nitric Oxide. Washington DC: Occupational Safety & Health Administration. (Available at:http://www.osha.gov/dts/chemicalsampling/data/CH_256700.html).
30. Westbrook CK, Dryer FL. Chemical kinetic modeling of hydrocarbon combustion. *Proc Energy Combust Sci*. 1984;10:1–57.
31. Lee CK, Singer AB, Barton PI. Global optimization of linear hybrid systems with explicit transitions. *Systems & Control Letts*. 2004;51: 363–375.
32. Singer AB, Barton PI. Bounding the solutions of parameter dependent nonlinear ordinary differential equations. *SIAM J on Scientific Computing*. 2006;27:2167–2182.
33. Singer AB, Barton PI. Global optimization with nonlinear ordinary differential equations. *J Global Optimization*. 2006;34:159–190.
34. Gill PE, Murray W, Saunders MA. SNOPT: An SQP Algorithm for large-scale constrained optimization. *SIAM Review*. 2005;47:99–131.
35. Tolsma J, Barton PI. DAEPACK: an open modeling environment for legacy models. *Ind & Eng Chem Res*. 2000;39:1826–1839. (Available at: http://yoric.mit.edu/daepack/daepack.html).
36. Galán S, Feehery WF, Barton PI. Parametric sensitivity functions for hybrid discrete/continuous systems. *Applied Numerical Mathematics*. 1999;31:17–47.
37. Feehery WF, Tolsma JE, Barton PI. Efficient sensitivity analysis of large-scale differential-algebraic systems. *Applied Numerical Mathematics*. 1997;25:41–54.
38. Tolsma JE, Barton PI. Hidden discontinuities and parametric sensitivity analysis. *SIAM J on Scientific Computing*. 2002;23:1861–1874.
39. Tolsma JE. Block solver manual (version 1.0) technical report. Process Systems Engineering Laboratory, Department of Chemical Engineering, Massachusetts Institute of Technology; 2000. (Available at: http://yoric.mit.edu/daepack/download/Manuals_Pres/blocksolver.ps).

Appendix: Equivalency of Minima of the Two-Stage Mathematical Program and its Single-Level Equivalent Program

The two-stage program

$$\begin{aligned}\min_{\mathbf{x}} \quad & f^{(1)}(\mathbf{x}) + \sum_{i=1}^{N_d} p_i Q_i \\ \text{s.t.} \quad & \mathbf{0} \geq \mathbf{g}^{(1)}(\mathbf{x}) \\ & \mathbf{0} = \mathbf{h}^{(1)}(\mathbf{x}) \\ & \left.\begin{aligned} Q_i = \min_{\mathbf{y}} \quad & f^{(2)}(\mathbf{x},\mathbf{y},\mathcal{P}_i) \\ \text{s.t.} \quad & \mathbf{0} \geq \mathbf{g}^{(2)}(\mathbf{x},\mathbf{y},\mathcal{P}_i) \\ & \mathbf{0} = \mathbf{h}^{(2)}(\mathbf{x},\mathbf{y},\mathcal{P}_i) \\ & \mathbf{y} \in Y \end{aligned}\right\} \forall i \in \mathcal{I} \\ & \mathbf{x} \in X\end{aligned}$$

is rewritten in the following form to emphasize the the dependence of the objective function value on the second-stage variables, $\mathbf{y}_i$

$$\begin{aligned}J_T = \min_{\mathbf{x},\mathbf{y}} \quad & f^{(1)}(\mathbf{x}) + \sum_{i=1}^{N_d} p_i f^{(2)}(\mathbf{x},\mathbf{y}_i,\mathcal{P}_i) \\ \text{s.t.} \quad & \mathbf{0} \geq \mathbf{g}^{(1)}(\mathbf{x}) \\ & \mathbf{0} = \mathbf{h}^{(1)}(\mathbf{x}) \\ & \left.\begin{aligned} \mathbf{y}_i \in \arg\min_{\mathbf{z}} \quad & f^{(2)}(\mathbf{x},\mathbf{z},\mathcal{P}_i) \\ \text{s.t.} \quad & \mathbf{0} \geq \mathbf{g}^{(2)}(\mathbf{x},\mathbf{z},\mathcal{P}_i) \\ & \mathbf{0} = \mathbf{h}^{(2)}(\mathbf{x},\mathbf{z},\mathcal{P}_i) \\ & \mathbf{z} \in Y \end{aligned}\right\} \forall i \in \mathcal{I} \\ & \mathbf{x} \in X \\ & \mathbf{y} \equiv (\mathbf{y}_1,\ldots,\mathbf{y}_{N_d}).\end{aligned} \tag{T}$$

where the sets X, Y are assumed to be nonempty and compact; all functions are continuous; $\mathcal{I}$ has finite cardinality N_d and $p_i \geq 0$ with $\sum_{i=1}^{N_d} p_i = 1$.

The equivalent single-stage formulation of (T) is

$$\begin{aligned}J_S = \min_{\mathbf{x},\mathbf{y}} \quad & f^{(1)}(\mathbf{x}) + \sum_{i=1}^{N_d} p_i f^{(2)}(\mathbf{x},\mathbf{y}_i,\mathcal{P}_i) \\ \text{s.t.} \quad & \left.\begin{aligned} & \mathbf{0} \geq \mathbf{g}^{(2)}(\mathbf{x},\mathbf{y}_i,\mathcal{P}_i) \\ & \mathbf{0} = \mathbf{h}^{(2)}(\mathbf{x},\mathbf{y}_i,\mathcal{P}_i) \\ & \mathbf{y}_i \in Y \end{aligned}\right\} \forall i \in \mathcal{J} \\ & \mathbf{y} \equiv (\mathbf{y}_1,\ldots,\mathbf{y}_{N_d}) \\ & \mathbf{0} \geq \mathbf{g}^{(1)}(\mathbf{x}) \\ & \mathbf{0} = \mathbf{h}^{(1)}(\mathbf{x}) \\ & \mathbf{x} \in X.\end{aligned} \tag{S}$$

Any feasible point ($\mathbf{x}$, $\mathbf{y}$) of (T) trivially satisfies the constraints of (S). If (S) is infeasible then (T) is also infeasible.

The feasible set of points of (T) and (S) are $D_{(T)}$ and $D_{(S)}$, respectively.

By convention, if a program is infeasible, the solution value of the program is $+\infty$. If the program is unbounded, the solution value is $-\infty$.

Proposition 1. *If* (S) *is feasible, then*

1. *the minimum of program* (S) *exists*,
2. *the optimal solution value (min or inf) of* (T) *is equal to the optimal solution value of* (S),
3. *the two-stage formulation* (T) *is feasible and the minimum of* (T) *exists*,
4. *the set of optimal solutions are the same.*

Proof.

1. For feasible (S), compactness of the sets X and Y and the continuity of the objective and constraint functions guarantee the existence of a minimum.

2. The optimal solution values J_T and J_S are equal:

(a) $J_T \geq J_S$

$D_{(S)} \supset D_{(T)}$ and the two programs have the same variables, and the same objective function. $J_T \geq J_S$ follows.

(b) $J_S \geq J_T$

Let$(\mathbf{x}^*,\mathbf{y}^*)$ be an optimal solution of (S). All constraints of (T) are satisfied except,

$$\mathbf{y}_i^* \in \arg\min_{\mathbf{z}\in Y}\{f^{(2)}(\mathbf{x}^*,\mathbf{z},\mathcal{P}_i) : \mathbf{0} \geq \mathbf{g}^{(2)}(\mathbf{x}^*,\mathbf{z},\mathcal{P}_i), \quad \mathbf{0} = \mathbf{h}^{(2)}(\mathbf{x}^*,\mathbf{z},\mathcal{P}_i)\}, \ \forall i \in \mathcal{J}. \quad \text{(A1)}$$

Let Eq. A1 not hold for some $j \in \mathcal{I}$. Still, $\mathbf{y}_j^*$ is feasible for the embedded program in Eq. A1, as it is an element of the optimal solution of (S) with $\mathbf{0} \geq \mathbf{g}^{(2)}(\mathbf{x}^*,\mathbf{y}^*_j,\mathcal{P}_j)$, $\mathbf{0} = \mathbf{h}^{(2)}(\mathbf{x}^*,\mathbf{y}_j*,\mathcal{P}_i)$. Either $\mathbf{y}_j*$ is the only feasible point hence an optimal solution or there exists $\bar{\mathbf{y}}_j \neq \mathbf{y}_j*$ such that $f^{(2)}(\mathbf{x}^*,\mathbf{y}_j*,\mathcal{P}_j) \geq f^{(2)}(\mathbf{x}^*,\bar{\mathbf{y}}_j,\mathcal{P}_j)$. If strict inequality holds, $(\mathbf{x}^*,\mathbf{y}^*)$ is not an optimal solution of (S). Hence, Eq. A1 holds and $(\mathbf{x}^*,\mathbf{y}^*)$ is feasible for (T). Since $(\mathbf{x}^*,\mathbf{y}^*)$ is optimal for (S), feasible for (T) and the objective functions are the same, $J_S \geq J_T$ follows.

3. If an optimal solution of (S) exists, (T) is feasible as proven. Since $J_S = J_T$, it directly follows that the minimum of (T) exists.

4. The set of optimal solutions arg min (T) and arg min (S) are equal.

(a) arg min (S) $\subset$ arg min (T)

Any optimal solution of (S) is feasible for (T). The objective functions of both programs, as well as optimal solution values are the same and the result follows.

(b) arg min (T) $\subset$ arg min (S)

An optimal solution of (T) is also feasible for (S). From the equality of the optimal solution values, an optimal solution of (T) is also an optimal solution of (S).

Discussion on Local Minimum of the Single-Stage Equivalent Formulation

Let $N_\varepsilon(\mathbf{x}^*,\mathbf{y}^*)$ a ball of radius ε centered at $\{\mathbf{x}^*,\mathbf{y}^*\}$. By definition, a local minimum $(\mathbf{x}^*,\mathbf{y}^*)$ of (S) satisfies

$$f^{(1)}(\mathbf{x}) + \sum_{i=1}^{N_d} p_i f^{(2)}(\mathbf{x},\mathbf{y}_i,\mathcal{P}_i) \geq f^{(1)}(\mathbf{x}^*) + \sum_{i=1}^{N_d} p_i f^{(2)}(\mathbf{x}^*,\mathbf{y}_i^*,\mathcal{P}_i), \quad \forall (\mathbf{x},\mathbf{y}) \in D_{(S)} \cap N_\epsilon(\mathbf{x}^*,\mathbf{y}^*). \quad \text{(A2)}$$

The constraint (A1) is not necessarily satisfied, since $\mathbf{y}_i*$ may not be an optimal solution of the program in (A1), for $\mathbf{x}^*$ except with the additional restriction that $\{\mathbf{x},\mathbf{y}\} \in D_{(S)} \bigcap N_\varepsilon(\mathbf{x}^*,\mathbf{y}^*)$. Hence, $\{\mathbf{x}^*,\mathbf{y}^*\}$ may not be feasible for (T), and it may not be a local minimum of (T).

The solutions of the program,

$$\begin{aligned} J_L = \min_{\mathbf{x},\mathbf{y}} \ & f^{(1)}(\mathbf{x}) + \sum_{i=1}^{N_d} p_i f^{(2)}(\mathbf{x},\mathbf{y}_i,\mathcal{P}_i) \\ & \left.\begin{aligned} \text{s.t. } \mathbf{y}_i \in \ & \text{arg local } \min_{\mathbf{z}} f^{(2)}(\mathbf{x},\mathbf{z},\mathcal{P}_i), \ \forall i \in \mathcal{J} \\ & \text{s.t. } \mathbf{0} \geq \mathbf{g}^{(2)}(\mathbf{x},\mathbf{z},\mathcal{P}_i) \\ & \quad \mathbf{0} = \mathbf{h}^{(2)}(\mathbf{x},\mathbf{z},\mathcal{P}_i) \\ & \quad \mathbf{z} \in Y \end{aligned}\right\} \forall i \in \mathcal{J} \\ & \mathbf{y} \equiv (\mathbf{y}_{(1)},\ldots,\mathbf{y}_{N_d}) \\ & \mathbf{0} \geq \mathbf{g}^{(1)}(\mathbf{x}) \\ & \mathbf{0} = \mathbf{h}^{(1)}(\mathbf{x}) \\ & \mathbf{x} \in X \end{aligned} \quad \text{(LS)}$$

where the operator arg local min returns the set of local minima of a program are considered next.

Proposition 2. *Let* $(\mathbf{x}^*,\mathbf{y}^*)$ *be a local minimum of* (S) *then it is feasible and a local solution for* (LS).

Proof. $(\mathbf{x}^*,\mathbf{y}^*)$ satisfies all constraints of (LS), hence, it is feasible and per (A2), it is a local minimum of (LS).

Manuscript received Dec. 21, 2006, revision received Aug. 9, 2007, and final revision received Dec. 29, 2007.